A 3-D-Printed Tactile Probe Based on Fiber Bragg Grating Sensors for Noninvasive Breast Cancer Identification

D. Lo Presti, *Member, IEEE*, A. Dimo, *Student Member, IEEE*, L. Zoboli, D. Bianchi, C. Massaroni, *Senior Member, IEEE*, V. Altomare, A. Grasso, C. M. Oddo, *Senior Member, IEEE*, A. Gizzi, *Senior Member, IEEE*, and E. Schena, *Senior Member, IEEE*

***Abstract*—Tissue palpation is one of the most popular techniques to detect tissue abnormalities in clinical scenarios, including breast examination. However, the tactile sensation used to identify tumors by the clinician or a woman during breast palpation makes this procedure subjective. Over the past decades, tactile sensors have been developed to quantitatively discriminate between cancerous and healthy tissues, but most of these systems still suffer from low force sensitivity, high power consumption, reduced sterilization durability, and electrical noise. This study aims to overcome these limitations by exploiting the advantages of fiber Bragg grating (FBG) technology combined with the ones of 3-D printing to develop an innovative tactile probe for breast cancer identification. FBGs have already been proposed for tissue palpation in minimally invasive surgery via tactile sensing, while their application in superficial palpation is still overlooked. To the best of authors' knowledge, this is the first work in which the FBG integration into 3-D-printed structures is proposed for breast superficial palpation. Here, we first focused on the sensing unit design optimization via finite-element analysis, fabrication, and metrological characterization. Then, the final prototype of the tactile probe integrating multiple identical sensing units was fabricated, and the results of tests on silicone samples with different hardness and on a phantom mimicking breast tissue with an early stage tumor were discussed. The promising findings will guide further optimization of the tactile probe design to improve system spatial resolution, reduce its encumbrance, and provide feedback to the user for applications on patients.**

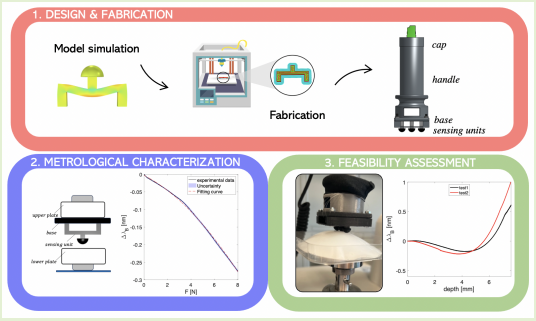

***Index Terms*—3-D printing, breast cancer, fiber Bragg gratings (FBGs), tactile sensing, tissue palpation.**

I. Introduction

TO DATE, one of the most widespread techniques to explore tissue abnormalities is represented by tissue palpation [1]. Tissue palpation is used in many fields of medicine and can be divided into methods to detect a suspicious area near the surface of the body noninvasively (i.e., surface palpation) or farther inside the body during minimally invasive surgery (MIS) [2], [3].

The detection of tissue abnormalities through surface palpation is expected to be particularly useful for breast cancer identification at the earliest stage since tumors alter the mechanical properties of tissue [4]. Breast cancer is the most frequent neoplasm by incidence in the female population and among the leading causes of death in women worldwide. It is estimated that one in eight women will be affected by this disease in their lifetime [5]. One of the main symptoms of breast cancer is the presence of a lump, and its early stage identification is crucial for increasing the chance of recovery and survival from the disease [6].

To date, clinical breast examination (CBE), ultrasound, mammography, and magnetic resonance imaging are among the most common methods for breast cancer screening and diagnosis [7], [8]. All these techniques require a specialist

Manuscript received 23 July 2023; revised 11 August 2023; accepted 11 August 2023. Date of publication 24 August 2023; date of current version 16 October 2023. The associate editor coordinating the review of this article and approving it for publication was Prof. Carlos Marques. *(Corresponding author: D. Lo Presti.)*

D. Lo Presti, A. Dimo, C. Massaroni, and E. Schena are with the Unit of Measurements and Biomedical Instrumentation, Università Campus Bio-Medico di Roma (UCBM), 00128 Rome, Italy (e-mail: d.lopresti@unicampus.it; a.dimo@alcampus.it; c.massaroni@unicampus.it; e.schena@unicampus.it).

L. Zoboli, D. Bianchi, and A. Gizzi are with the Unit of Nonlinear Physics and Mathematical Models, Università Campus Bio-Medico di Roma (UCBM), 00128 Rome, Italy (e-mail: l.zoboli@unicampus.it; d.bianchi@unicampus.it; a.gizzi@unicampus.it).

V. Altomare and A. Grasso are with the Breast Surgery Unit, Campus Bio-Medico University Hospital Foundation, 00128 Rome, Italy (e-mail: v.altomare@policlinicocampus.it; a.grasso@policlinicocampus.it).

C. M. Oddo is with the Biorobotics Institute, Department of Excellence in Robotics and AI, and the Interdisciplinary Research Center "Health Science," Scuola Superiore Sant'Anna, 56025 Pontedera, Italy (e-mail: calogero.oddo@santannapisa.it).

Digital Object Identifier 10.1109/JSEN.2023.3306970

to perform correctly and, given the high number of women undergoing screening annually, require a large number of allocated resources and time with substantial healthcare costs [9]. In addition to these methods, doctors recommend women to perform self-palpation once a month [10]. For this reason, self-examination is often considered the first tool in the prevention of breast cancer [11]. Self-palpation allows a woman to learn about the structure and general appearance of the breast to better discover any unusual changes [11]. Unfortunately, breast palpation has been hampered by problems inherent in subjectivity and dependence on the examiner's experience [12], [13], [14].

Therefore, patients and physicians can benefit from the development of sensorized devices for a quantitative evaluation of changes in tissue stiffness to increase the probability of finding an early stage tumor [14]. Indeed, both benign and cancerous tumors have a significantly higher Young's modulus (E) than that of healthy soft tissues [15], [16].

In the last decades, several tactile probes have been developed to guide the physician or self-user in the noninvasive detection of breast cancers [3], [17], [18]. Most integrate capacitive, piezoresistive, and piezoelectric sensors for tissue hardness or elasticity determination. For example, Won et al. [3] proposed a compact haptic imaging system consisting of piezoelectric sensors arranged in an array configuration to measure force distribution on breast models and human subjects. However, the probe has some disadvantages, like low force sensitivity and the consumption of a great deal of power. These shortcomings, together with less durability to sterilization and many output wires, can be considered the main limitations of traditional palpation sensors.

To overcome these issues, this work proposed a novel tactile probe for breast palpation, with the aim of identifying tumors by discriminating tissues with different stiffness. Specifically, the device exploits the advantages of fiber Bragg grating (FBG) technology integrated into a 3-D-printed structure. The FBG integration during 3-D printing combines the innumerable benefits of fiber optic technology (e.g., compactness, immunity to electromagnetic interference, not electrical in nature, multiplexing capability, and high metrological properties) [19] with those of rapid prototyping (e.g., low cost, high possibility of customizing the device to be printed, and low manufacturing times) [20], [21]. FBGs have already been used to develop tactile sensors for tissue palpation in the literature, but their application was mainly limited to MIS [22], [23], [24], [25], [26]. Indeed, to the best of authors' knowledge, this is the first work in which FBG and 3-D-printing technologies are joined together for the noninvasive palpation of the breast.

In the following sections, a focus on the core sensing of the tactile probe is proposed starting from the description of the sensing principle, the design of the sensing unit, and its modeling via a finite-element analysis (FEA) to optimize the FBG positioning within the structure, and the manufacturing process proposed to embed FBG during 3-D printing (Section II). Then, the metrological properties of the developed sensing unit are investigated, followed by tests on silicone samples with different hardness (Section III). Finally, the tactile probe instrumented by three identical sensing units is developed and tested on a silicone phantom mimicking a breast tissue with a cancer to check the system capability of detecting a tumor by investigating multiple measurement sites, simultaneously (Section IV).

II. Sensing Unit: Sensing Principle, Design, Model Simulation, and Fabrication

A. Sensing Principle

An FBG sensor is made by laterally exposing the core of a single-mode optical fiber to an intense UV laser light to form a period refractive index modulation called grating [19]. When a broadband light source illuminates the FBG, it reflects a specific wavelength known as Bragg wavelength (λ_B) and transmits all the other ones. The λ_B is defined as

$$\lambda_B = 2n_{\text{eff}}\Lambda \tag{1}$$

where n_{eff} is the effective refractive index of the fiber core, and Λ is the grating period. Both these parameters change when the FBG is exposed to strain (ε) and temperature variations (ΔT) as

$$\Delta\lambda_B = \lambda_B(1 - p_e)\varepsilon + (\alpha + \zeta)\Delta T \tag{2}$$

where $\Delta\lambda_B$ is the shift of λ_B experienced by the FBG, p_e is the strain-optic coefficient, α is the thermal expansion coefficient, and ζ is the thermo-optic coefficient of the silica.

Once integrated into an external substrate, the FBG response to physical inputs can change in accordance with the properties of the material used to embed the grating [19], [27], [28], [29], [30], [31], [32].

As shown in (2), an FBG is intrinsically sensitive to ε and temperature (T), but when integrated into ad hoc designed structures can be sensitive to additional parameters, including relative humidity (RH) and force (F).

In this study, we proposed a U-shaped structure with paralleled flanges and a semispherical head for breast palpation. The chosen design is expected to enable the transduction of the F applied on the head into a longitudinal ε on the FBG at the specimen core. Here, TPU 95A was used as printing material for its high flexibility compared to other filaments, availability, and usability [33], [34]. Fig. 1 shows the schematic of the sensing unit with its working principle.

Once the FBG is integrated into the web section of the U-structure and an F is applied to the contact head (see Fig. 1), the U-structure experiences a deflection. In particular, if we consider this framework as a beam-like structure, we should expect that the top surface of the structure is compressed and the bottom surface is tensioned, as shown in Fig. 1. Hence, the compression stresses from the top gradually reduce to zero, and then, the tension starts and increases from zero toward its maximum value at the bottom of the structure. The point at which this switch occurs is called the neutral axis. Hence, when an FBG sensor is embedded into the proposed structural design, it will experience a deformation in accordance with the body deflection under loading conditions: a positive $\Delta\lambda_B$ is expected to be experienced by the FBG when it is placed where the structure is in tension while a negative

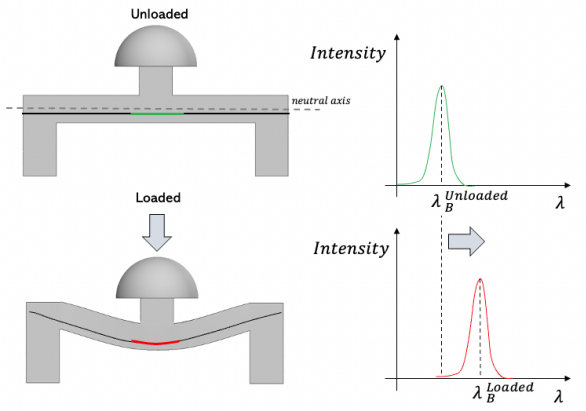

Fig. 1. Sensing principle of an FBG sensor integrated under the neutral axis. A red shift is experienced by the sensor under loading conditions since tension stresses occur in the body part where the grating is embedded.

$\Delta\lambda_B$ where in compression. In addition, this effect is expected to be emphasized when the structure is pushed against stiffer surfaces like breast tumors. However, the proposed design shows some structural modifications compared to a beam (i.e., the presence of two lateral columns, also called flanges, and a central column between the web and the head).

Moreover, the sensor is not free to slide while working but is intended to be fixed on an external support (i.e., the base) to apply F during tissue palpation. These structural modifications and working conditions may cause changes in its mechanical response. Hence, an FEA was conducted to better investigate this aspect before the sensor fabrication and optimize the sensor positioning within the structure to guarantee a good tradeoff between the sensing performance and FBG robustness.

B. FEA and Sensor Positioning Optimization

To investigate the mechanical response of the designed sensor when a load is applied on top of the head, two finite-element (FE) models have been built [Fig. 2(a)]. We investigated the behavior of the proposed sensor design when it is free to have lateral sliding and when it is fixed into a structure. In both models, the same Cartesian global coordinate system $\{O, x, y, z\}$, where z is the vertical axis, has been adopted as a reference frame. In more detail, a roller model has been used to simulate free lateral sliding when the sensor is not inserted in the supporting base. In this model, vertical displacements ($u_z = 0$) are restrained on the lowermost faces, and simultaneously, one edge of these faces is fixed (i.e., $u_x = u_y = u_z = 0$) to prevent rigid motion (Fig. 2(a), blue boundary condition). On the one hand, a fixed model (Fig. 2(a), red boundary condition) has been used to assess the behavior of the sensor inserted in the base, which means that the lateral columns of the U-body are prevented from sliding outward when a force F is applied on the head; specifically, the presence of the external supporting base is modeled as fixed constraints (i.e., $u_x = u_y = u_z = 0$) prescribed on the bottom faces of the lateral columns, and a downward force $F = 8N$ has been applied. Both FE models have been discretized with a quadratic tetrahedral mesh of 433 154 nodes and 1 796 568 degrees of freedom (DOFs).

The simulations have been carried out within the FE environment COMSOL Multiphysics 5.6. The strain $\varepsilon_y(s)$, where $s \in [0, b]$, has been investigated on five parallel paths aligned with the y-direction and distanced $\delta = 0.2$ mm along the z-axis. In detail, the starting and ending points of the lowermost path are $(x, y, z) = (0, -b/2, a1 - a2/2 - 2\delta)$ and $(x, y, z) = (0, b/2, a1 - a2/2 - 2\delta)$, and the successive paths are obtained by shifting the z-coordinate of these points by δ.

As depicted in Fig. 2(b), the response of the structure near the beginning and ending of the paths is greatly affected by the presence of the two lateral columns acting as added inertia to the cross section of the device and inhibiting free bending. The central column is instead responsible for the peculiar behavior of ε_y at the center of the paths, where many paths experience compression instead of being in tension as would be expected. This is because, under the action of the external force, the central column undergoes a barreling effect and exerts a shrinking action (compression) on the horizontal span of the U-structure. This local compression occurs in both models but less markedly in the free-sliding model [Fig. 2(b) and (c)], as the path crossing the horizontal span at precisely half its height experiences compression in the fixed 3-D model while being in tension in the free-sliding one.

Considering the FEA results, the strain distribution along the cutlines shown in Fig. 2(b) reached values that may induce breakage of the FBG sensor. However, the FE model has not considered the bonding interactions established at the interface between the fiber optic sensor and the 3-D-printed material during the printing. Some recent studies showed that an external substrate dampens the strain level experienced by an FBG sensor placed at the specimen core with respect to a nonencapsulated sensor [35], [36]. Hence, we decided to place the optical fiber along the light blue cutline since it can guarantee the optical fiber to be entirely under tensile loading conditions, even if it may experience compression when integrated into the base, as shown in Fig. 2(b).

C. Structural Design and Geometrical Features of the Sensing Unit

The proposed sensor is intended to work by pushing the breast surface to discriminate cancerous from healthy tissue by detecting differences in terms of their stiffness. To accomplish this aim, the structural design of the sensing unit consists of a U-shaped body with a central column, an FBG sensor (λ_B of 1541 nm, 10 mm of grating length, and reflectivity >90%; commercialized by AtGrating Technologies, Shenzhen, China) made of silica and acrylate-recoated integrated into the structure, and a hemispherical contact head. The main dimensions of the sensing unit are shown in Fig. 3.

The connection between the central column of the U-structure and the head is made by cyanoacrylate glue, and the integration of the FBG during printing is carried out thanks to the design of a grooved channel centered at the middle of the web (Fig. 3). According to the FE results in Fig. 2(b) and (c), the sensor is also designed to fit a base by integrating its flanges for a depth of 3 mm, as shown in Fig. 4. A joint interconnection is formed between the two flanges and the base.

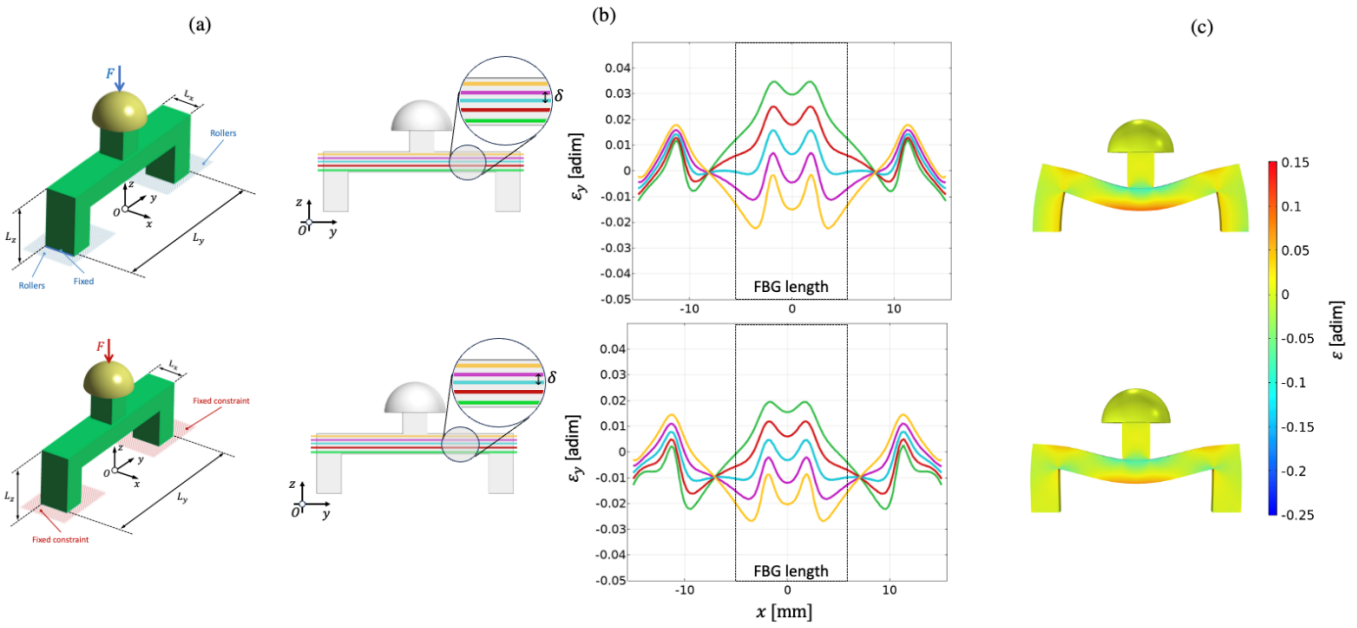

Fig. 2. (a) FE models for the study of the deflection under an applied force: roller model (boundary condition in blue) and fixed model (boundary condition in red). (b) Strain evolution in fiber direction on cut lines: roller configuration (above) and fixed configuration (below) with a shadow indicating the 10 mm of FBG length. (c) Strain map in fiber direction: roller configuration (above) and fixed configuration (below).

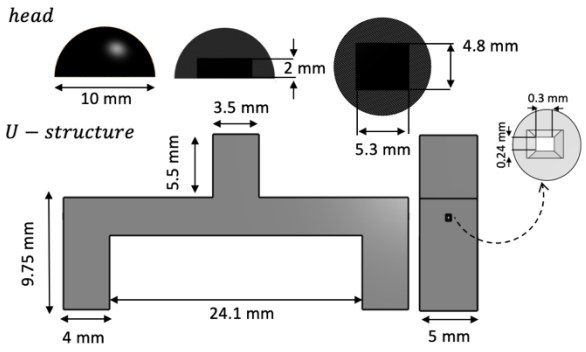

Fig. 3. Dimensional characteristics of the 3-D-printed sensing unit consisting of a semispherical head and a U-structure with a channel for the FBG embedment.

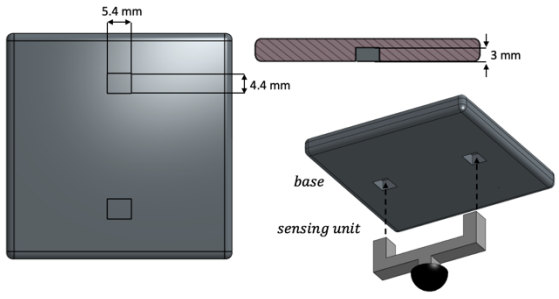

Fig. 4. Base where the sensing unit is intended to be fit for force application in the experimental characterization.

D. Fabrication Process of the Sensing Unit

All the components of the sensing unit were printed using the fused deposition modeling method. The contact head was printed in polylactic acid (PLA) to be more rigid than the U-structure in which the sensor is placed, made of TPU 95A. In this way, a full transmission of the entire F applied on the head to the U-structure and, in turn, to the FBG can be achieved. The main fabrication steps of the U-structure with the sensorized web are listed in the following.

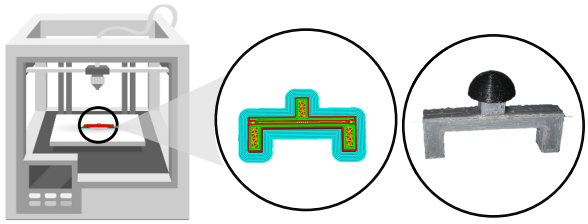

Fig. 5. Fabrication step with a zoom on the printed layer (i.e., the 21st one) with the channel for the FBG embedment and the final prototype of the 3-D-printed sensing unit.

1) Preprocessing: It consists of the generation of the *g.code* file of the computer aided design using CURA slicing software, setting an infill density of 100%, a triangle pattern, and a print speed of 30 mm/s. Then, the job is sent to the 3-D printer (Creality Ender v3, Creality, Shenzhen, China).

2) Production: The printing starts. The melted filament (i.e., TPU 95A, Sunlu, Shenzhen, China) is extruded by the nozzle and deposited layer by layer on the printer plate. At the 21st layer, the channel to embed the optical fiber is created (see Fig. 5). The printer is stopped, and the optical fiber is pretensioned into the channel. The printer is resumed.

3) Postprocessing: At the end of the process, the U-structure integrating the FBG during printing is removed from the plate, the head printed in PLA is attached to the structure, and the sensor is ready to fit in the base.

III. Metrological Characterization and Tests on Silicon Substrates

In this section, we investigated the metrological properties of the proposed sensing unit with particular regards toward

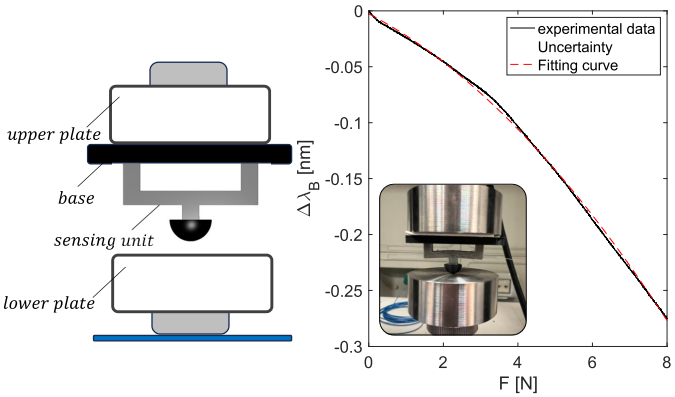

Fig. 6. Scheme and photograph of the 3-D-printed sensor placed between the upper and lower plates of the compression machine are also included with the $\Delta\lambda_B$ versus F experimental data (black line) with the fitting curve (red line) and the expanded uncertainty (blue shadow area).

its response to F and T inputs. Then, the sensing unit capability of discriminating materials with a different stiffness was assessed.

A. Metrological Characterization

1) Response to Force: After the fabrication process, a metrological characterization was performed to assess the response of the developed sensing units under loading conditions. We chose a range of F from ~0 to 8 N and performed compression tests with the sensing unit joining the base and attached to the upper plate of a compression testing machine (Instron 3365), as shown in the following.

The experimental setup consists of a testing machine (Instron mod. 3365), the sensor positioned on the machine plate, and an optical interrogator (si255 Micron Optics) to record the output of the embedded FBG at 100 Hz. To investigate the response to F and assess its repeatability, eight repetitions were performed at quasi-static conditions by setting a velocity of 2 mm/min. The recorded data were analyzed in MATLAB environment to obtain the calibration curve ($\Delta\lambda_B$ versus F) by averaging the $\Delta\lambda_B$ versus F curves resulting from the eight repetitions. The expanded uncertainty was also estimated by considering a t-Student distribution with a level of confidence of 95% and a number of DOFs equal to seven. Fig. 6 shows the response of the developed sensor to F. The curve that best fits the experimental trend is a second-order polynomial curve. Hence, to find out the value of F sensitivity, we used the following equation:

$$S_F^{\text{mean}} = \frac{\Delta\lambda_B(F^{\max}) - \Delta\lambda_B(F^0)}{F^{\max} - F^0} \tag{3}$$

where S_F^{mean} represents the average sensitivity to F, $\Delta\lambda_B(F^{\max})$ is the value of $\Delta\lambda_B$ at 8 N, and $\Delta\lambda_B(F^0)$ is the value of $\Delta\lambda_B$ at ~0 N. By using (4), an S_F^{mean} value of −0.06 nm/N was found. Moreover, results showed a low measurement uncertainty across the eight tests (thin shadow area in Fig. 6), suggesting high repeatability in the sensor response.

As shown in Fig. 6, a reduction of $\Delta\lambda_B$ with F is experienced by the developed sensor. This trend is in line with the FE results in Section II-B, suggesting that a compression is experienced by the FBG sensor under loading conditions in the F range ~0–8 N. Moreover, the $\Delta\lambda_B(F^{\max})$ is −0.27 nm. It corresponds to a ε_y of 2.3×10^{-4} since the strain sensitivity of the not-encapsulated FBG is 1.2 nm/mε. This result is approximately two orders of magnitude lower than the modeled one in Fig. 2(b), underlining the damping effect caused by the fiber structure interactions. However, the S_F^{mean} value obtained in this study is higher than the ones of similar systems based on the same technology but integrated into elastomers [38], [39], [40], [41], suggesting a stronger adhesion between the FBG and 3-D-printed filaments.

2) Response to Temperature: As shown in (2), an FBG sensor is intrinsically sensitive to T. Hence, the influence of ΔT was also investigated to understand how the thermal properties of the external substrate will affect the FBG response to F. Indeed, a thermal expansion of the material that embeds the grating can cause thermal-induced ε on the FBG output.

A laboratory oven was used to expose the developed sensor to a controlled ΔT. A thermal probe was used to record T reference values, while the output changes of the FBG were recorded using an FBG interrogator (si255 Micron Optics) at a sampling rate of 10 Hz. A single repetition was carried out as follows: the sensor and the reference instrument were placed within the oven and a T of 40 °C was set. Once this value of T was reached, we waited for 30 min to allow the sensor to reach the equilibrium before switching off the oven to guarantee a static condition and cool down the sensors up to the environmental T (i.e., ~22 °C). The sensitivity to T (S_T) was evaluated considering the descending phase where T ranged from 40 °C to ~22 °C (i.e., the ambient T value). Results showed a nonlinear response that can be fit using a second-order polynomial curve, as shown in Fig. 7. It is worth knowing that a nonencapsulated FBG sensor has a linear response to T with an S_T value of 0.01 nm/°C. Here, we found a nonlinear behavior with an average $S_T(S_T^{\text{mean}})$ of 0.05 nm/°C considering the range of interest (i.e., from ~22 °C to ~40 °C), evaluated as follows:

$$S_T^{\text{mean}} = \frac{\Delta\lambda_B(\Delta T^{\max}) - \Delta\lambda_B(\Delta T^0)}{T^{\max} - T^0} \tag{4}$$

with $\Delta\lambda_B(T^{\max})$, the value of $\Delta\lambda_B$ at 40 °C, and $\Delta\lambda_B(T^0)$, the value of $\Delta\lambda_B$ at ~22 °C. A value of S_T^{mean} higher than the one of the nonencapsulated FBGs (0.05 versus 0.01 nm/°C) suggests that the thermal expansion of the TPU material causes an additional strain on the encapsulated grating.

However, when the tactile probe integrating the sensing unit will be used in the scenario of interest, the thermal influence on the FBG output can be considered negligible since the sensing 0.05 unit integrated into the TPU material will not be in direct contact with the body, but the tissue under investigation will be pushed by the head in PLA.

B. Application on Silicones With a Different Stiffness

A tactile probe for recognizing breast cancer from the body surface should be able to discriminate tissues with different mechanical properties. Hence, we investigated the capability of the sensing unit of discriminating silicones with different stiffness.

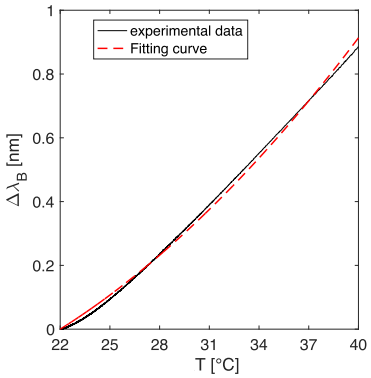

Fig. 7. $\Delta\lambda_B$ versus T experimental data (black line) and the fitting curve (red line).

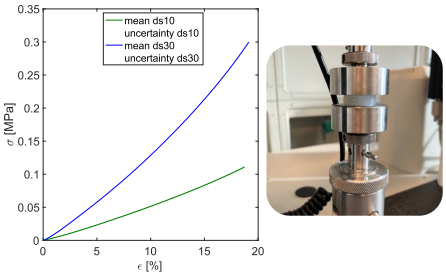

Fig. 8. Average σ versus ε curve of ds10 (green line) with the related uncertainty (green shadow area) and of ds30 (blue line) with the related uncertainty (blue shadow area).

1) Silicone Rubbers Young's Modulus: To assess the sensor capability of discriminating materials with different stiffness, two cylindrical specimens made of silicone rubber (i.e., Dragon Skin 10A—ds10, more flexible, and Dragon Skin 30A—ds30, more rigid) were fabricated.

From the technical bulletins of the bicomponent silicones, ds10 has a Shore hardness of 10 A and ds30 has a Shore hardness of 30 A, but no additional information about the value of the Young's Modulus (E) is included. Hence, we first performed compression tests on the silicone materials to estimate the E of ds10 and ds30.

By following the ISO 7743:2017 standard [37], we defined the shape and dimensions of the silicone samples: cylinders with a diameter of 29 mm and a height of 12.5 mm. To shape the silicones, two molds were printed in PLA, and Dragon Skin materials were cast inside the molds after mixing the two components and degassing the mixture to remove air bubbles. The curing stage lasted 5 h for ds10 and 16 h for ds30 before removing the cylinder shaped silicones from the mold. A number of four compression tests were carried out along the z-direction at a speed of 10 mm/min until a strain of ∼20% was reached. The average stress versus strain (σ versus ε) curve was obtained together with the estimation of the expanded uncertainty using a t-Student distribution with 95% of level of confidence and three DOFs (see Fig. 8). Results showed an E value of 0.55 MPa for ds10 and 1.41 MPa for ds30, confirming the higher (approximately three times) stiffness of ds30 than ds10.

2) Test of the Silicone Samples: Finally, to assess the sensing unit capacities of discriminating materials with different stiffness, we performed tests on the developed silicone samples as follows. The sensing unit fit the base and was stuck to the upper plate of the compression testing machine, and the silicone samples were positioned on the lower plate. A number of four consecutive compression tests were carried out by indenting the sensing unit for a depth of ∼5 mm in the silicone sample at a speed of 2 mm/min.

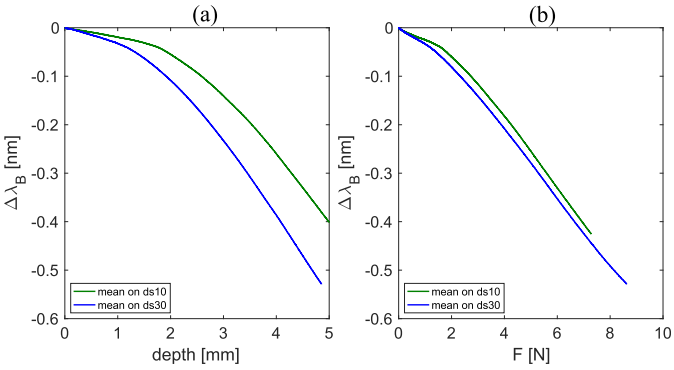

Fig. 9. Response of the sensing unit applied on ds10 (green line) and ds30 (blue line) in terms of: (a) $\Delta\lambda_B$ versus depth and (b) $\Delta\lambda_B$ versus F.

For each test, the output of the testing machine and the ones of the FBG sensor were recorded at a sampling rate of 100 Hz. The mean responses $\Delta\lambda_B$ versus depth and $\Delta\lambda_B$ versus F were obtained, as shown in Fig. 9. As clearly visible in the trends in Fig. 9(a) and (b), the sensor showed a higher $\Delta\lambda_B$ when compressed on ds30 (blue line for ds 30 and green line for ds10) since the ds30 sample has a higher stiffness than ds10 (as testified by the E values). Moreover, the average F value recorded by the testing machine confirmed these results [see Fig. 9(b)]: a higher F was reached during the tests on ds30 than during the ones on ds10, with the same indention depth (i.e., ∼5 mm). These findings suggest the high potentiality of the proposed sensing unit to discriminate materials with a different stiffness.

IV. Tactile Probe: Design, Fabrication, and Tests on a Phantom

After performing the metrological characterization and tests on silicone substrates with a different stiffness, we developed the tactile probe. In this study, we chose to integrate three nominally identical sensing units into the probe. In this way, the device will be able to investigate a total of three measurement sites simultaneously.

A. Components of the Tactile Probe

The probe is mainly composed of multiple sensing units (i.e., three 3-D-printed sensors based on FBG technology), a cover and a base with a screw thread connection to protect the sensors with the exception of their contact heads, and a fixed handle to allow the user an easier application of the pressure on the tissue. Finally, a cap with three apertures allowed installing the optical fiber *LC* adapters to enable the interconnection of the sensing units integrated into the tactile device to the FBG interrogator [see Fig. 10(a) and (b)]. The three sensing units are located one at the center of the base

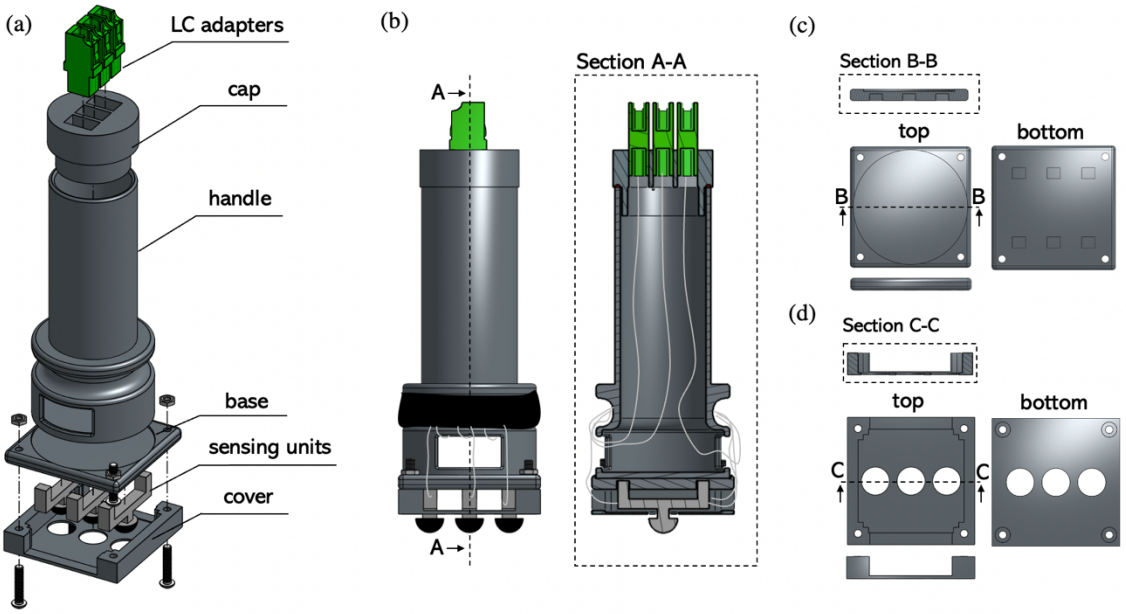

Fig. 10. (a) Schematic diagram of the tactile probe with the three sensing units inside the housing frame composed of the cover, the base, the handle and the cap for making easier the device usage in tissue palpation. (b) Cross-sectional view (section A–A) of the tactile probe to show the handle inner part with the optical fibers joining the *LC*-adapters. (c) and (d) Top, bottom, lateral cross views (Section B–B and Section C–C) of the base and the cover structures.

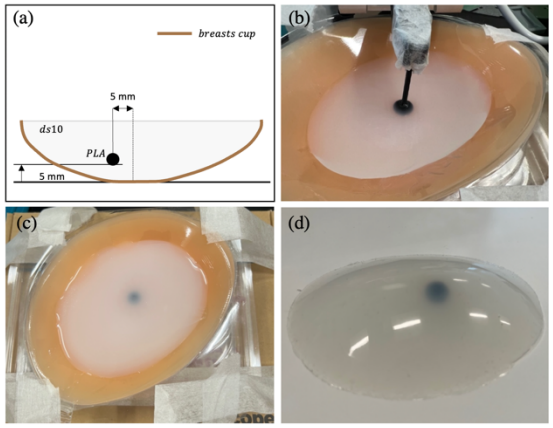

Fig. 11. (a) Design of the phantom. Fabrication steps: (b) from the PLA sphere positioning; (c) to the silicone curing; and (d) phantom peeling out from the cup.

and the others on its sides. As already described, a single FBG is embedded into each sensing unit along its neutral axis while the resting part of the optical fiber is first looped around the handle axle, similar to a spool, and then inserted through the handle to reach the adapter and mate the *LC* connector at the fiber end to the one of the patch cords [see Fig. 10(b)]. All the components of the probe are fabricated in PLA with the exception of the U-structure of the sensing units made of TPU. The main constitutive components of the probe with the dimensions are detailed in the following.

1) *The Cap:* The cap has an external diameter of 35 mm, an internal diameter of 28.7 mm, and an overall length of 23 mm. The cap is inserted into the handle for a height of 10 mm.
2) *The Handle:* The handle has an external diameter of 33.7 mm, an internal diameter of 30 mm, and an overall height of 103 mm. The handle is inserted into the base through a circular cavity designed on the top side of the base for a length of 1 mm.
3) *The Base:* The base has the same structure already described in Section II-B. It has a square shape with a length of 50 mm and a thickness of 5 mm. To fit the three sensing units on the bottom side, four additional rectangular cavities with a length of 5.4 mm and a width of 4.4 mm were designed compared to the previous structure [see Fig. 10(c)].
4) *The Sensing Units:* Three nominally identical sensors were integrated into the tactile probe on the bottom side of the base. The structural design and fabrication process are the ones described in Section II. The distance between the heads of close sensors is 12.55 mm.
5) *The Cover:* The cover has a square shape with a length of 50 mm and a height of 8.7 mm. It has a cavity for embedding the sensing units, with a width of 32.4 mm and a height of 7.5 mm. Moreover, three holes are designed to allow the sensors contact heads to peer out from the bottom side of the cover [see Fig. 10(c)]. In this way, the force can be applied to the breast skin surface on three contact points to investigate the presence of tissues with different hardness.

B. Application on a Silicone Phantom of a Breast With a Tumor Inside

To better investigate the capability of the proposed tactile probe in discriminating materials with different stiffness for application in breast cancer identification, a silicone phantom was developed [Fig. 11(a)], as detailed in the following. Then,

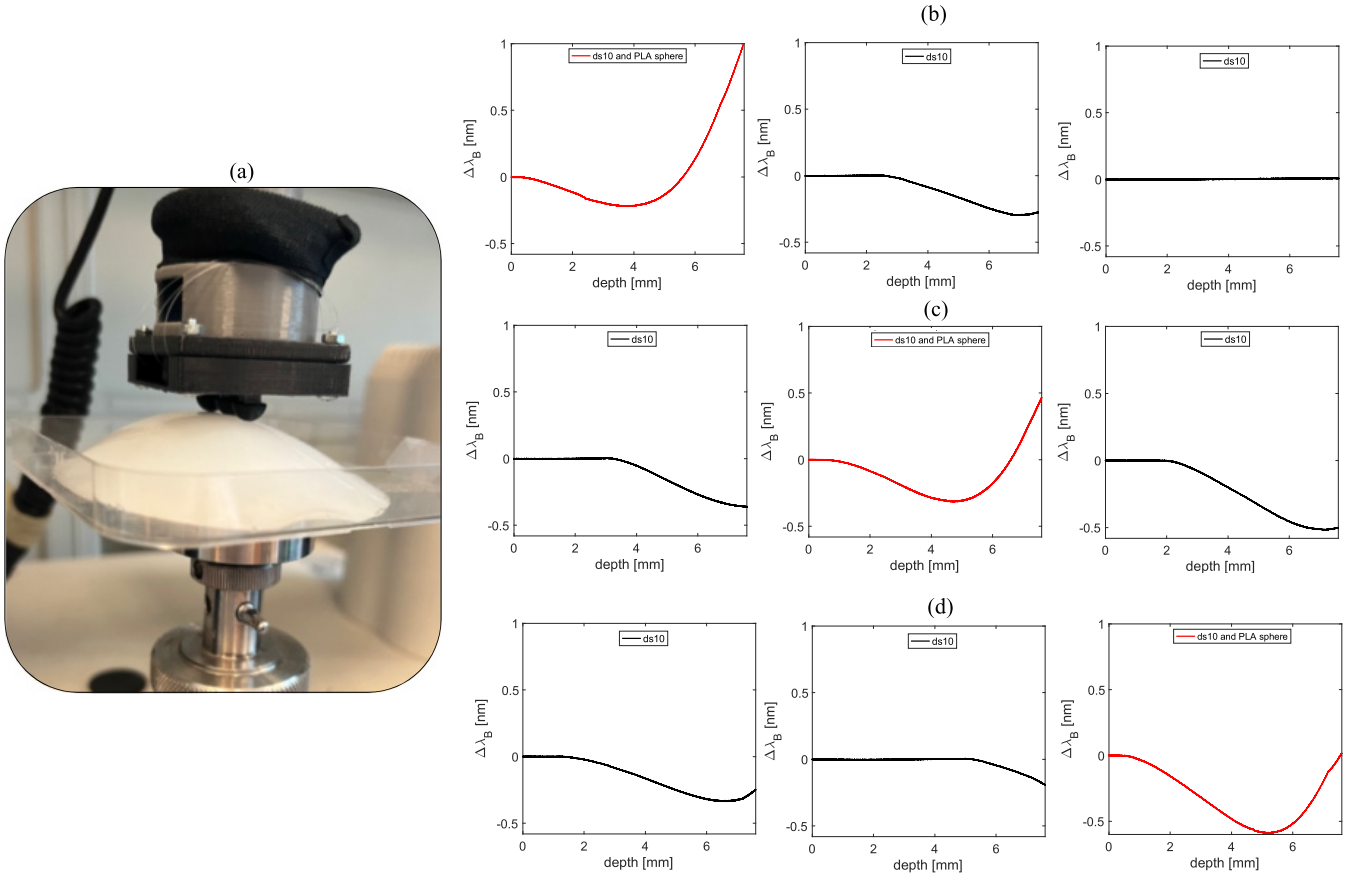

Fig. 12. (a) Photograph of the tactile probe pushing the phantom. (b)–(d) $\Delta\lambda_B$ versus depth trends: each row refers to a downward motion; in each, the trends in a black line refer to the two sensors not in contact with the ds10 surface without the PLA sphere, while the trend in a red line is related to the sensor which is pushing the area with the PLA sphere.

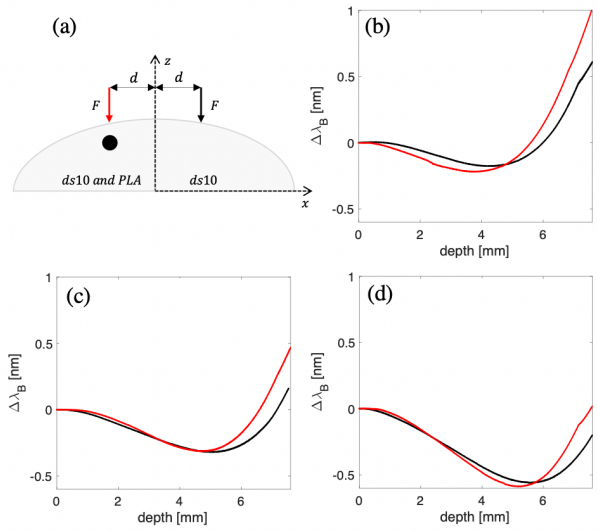

Fig. 13. (a) Schematic representation of the contact points of each sensing unit. (b)–(d) Trend $\Delta\lambda_B$ versus depth of each sensing unit when pushed on ds10 with PLA sphere (red line) and without PLA sphere (black line) while guaranteeing the same contact conditions.

preliminary tests were carried out to establish whether the palpation probe could detect the presence of the tumor when pushed against the surface of the phantom integrating a breast cancer model.

The design and fabrication stages of the silicone phantom with a breast cancer model are detailed in the following.

1) The breast tissue was made of ds10. The silicone was prepared according to the manufacturer's instruction and poured into a silicone breast lift cup to shape ds10 as the human breast [see Fig. 11(b) and (c)].
2) To emphasize the difference in terms of E between healthy tissue and cancer, a 3-D-printed sphere made of PLA was used to model a breast cancer. A diameter of 10 mm was used to mimic a tumor at the early stage.
3) The breast cancer model was inserted into the ds10 silicone matrix for a depth of ∼5 mm.
4) After a curing time of 5 h, the phantom is ready to be removed from the cup [see Fig. 11(d)].

The tactile probe capability of detecting the presence of a breast cancer model within the phantom was investigated using the compression machine already employed for the metrological assessment. In these experiments, the handle of the tactile probe was clamped by the upper grid and pushed against the phantom placed on the lower plate.

The performed protocol consists of two tests per sensing unit. In the first test, each sensing unit is consecutively pushed against the phantom exactly on the silicone area covering the PLA sphere [Fig. 12(a)]. In more detail, three straight downward motions are performed to allow each of the three sensors to be pushed against the silicone area covering the PLA sphere once. During each downward motion, only one sensor is expected to push the area with the tumor-like sphere [see Fig. 12(b)].

Then, the tactile probe is lifted up, and the phantom is adjusted to allow another sensor to push the silicone area covering the PLA sphere.

Fig. 12(b) shows the response of each sensor during the downward motions while pushing the phantom. As clearly highlighted by the trends, once the sensing unit pushed the ds10 in the area encapsulating the PLA sphere, an inflection point occurs at the level where the breast cancer model is located (∼4.5 mm). Moreover, a higher excursion in terms of $\Delta\lambda_B$ was found in each trend of the sensor pushing the area with the PLA sphere. However, the convex upper surface profile of the silicone phantom may lead to a different contact angle between each of the three sensing units and the ds10 surface that can be responsible for this behavior. For this reason, we performed an additional test. To guarantee the same contact conditions and, in turn, check if the differences in the trend in Fig. 12(b) are mainly due to the presence of a stiffer material than to the convex upper surface profile of the phantom, each sensing unit was pushed against a specular part of the phantom only made of ds10 at the same distance of the part made of ds10 and PLA sphere from the z-axis [Fig. 13(a)].

As shown in Fig. 13(b)–(d), each sensing unit reached the highest $\Delta\lambda_B$ in the presence of the tumor model. Moreover, the inflection points in all the trends in the presence of the tumor occur earlier than those in the absence of the tumor, suggesting the promising capacity of the tactile probe in identifying changes in the tissue properties.

V. Discussion and Conclusion

In this article, we presented a novel 3-D-printed FBG-based tactile probe for guiding the clinician or the self-user in the noninvasive detection of tumors in breast tissue. The prototype consists of three sensing units integrated into a probe to be easily handled by the user for applying F on multiple measurement sites simultaneously.

FEA guided the definition of a proper shape and modeled the sensing unit behavior as a force sensor. Fused deposition modeling (FDM) was used as a fabrication method to integrate the FBG during 3-D printing for this purpose, making the optical fiber more robust and easily deformed under loading conditions. Then, the metrological properties of the sensing unit were investigated, focusing on the sensor response to F and T. Results showed a negligible influence of T and high S_F values compared to other FBG-based force sensors already proposed in the literature for medical applications suggesting a stronger adhesion between the FBG and 3-D-printing filaments than between FBG and silicone rubbers or elastomers [38], [39], [40], [41]. Tests on silicone samples with different hardness (i.e., ds10 and ds30) showed the high capability of the developed sensing unit to discriminate materials with different mechanical properties. In addition, preliminary tests of the tactile probe were carried out on a phantom mimicking a breast cancer composed of ds10 with a harder spherical inclusion made of PLA with a diameter of 5 mm buried 5 mm under the phantom surface. The results proved the good performance of the proposed device in identifying the PLA sphere, as shown in Figs. 12 and 13.

To date, only a few solutions have been commercialized for breast tissue palpation. The most used are silicone pads developed to reduce friction between the fingers and the breast and help women during self-palpation, but no sensors are integrated into the silicone matrix to automatically detect tissue abnormalities. Other devices are based on ultrasound and pressure sensing modalities, but the low resolution often associated with these devices proposed is still limiting their widespread use [42], [43]. Hence, highly solved and sensitive multisensor configurations should be developed to overcome these shortcomings.

In the literature, most of the solutions for tactile sensing are based on electrical and piezoelectrical sensors. As in this study, an array configuration is usually preferred to investigate multiple measurement sites simultaneously [3], [17], [18]. Although more sensing units are integrated into these systems with respect to our device, these systems often have low sensitivity to F, are prone to electrical noise, and require high voltage, especially when piezoelectricity is exploited for tactile sensing.

These limits can be overcome by our tactile probe that exploits the unique advantages of FBG technology combined with the ones of FDM. Indeed, FBGs are small and compact and are inscribed into the core of an optical fiber that works by carrying light. No electrical voltages and disturbances are expected to occur with this kind of technology. In addition, integrating the FBG into a 3-D-printed structure makes the sensor more robust than sensing solutions into silicone matrices and easier to sterilize than other devices in the literature. The use of FDM also plays a crucial role in the FBG sensor performance since a better adhesion is expected to occur than silicones, and an FEA-guided optimization can be easily adopted by customizing printing settings and materials, thus reducing time and costs. However, FE models are often simplified since some interactions are difficult to characterize, such as the bond and interface shear on the fiber matrix interfacial surface. Hence, a simplified FEA can guide the sensor design, and then, the experimental results can also be used to fine-tune model parameters accordingly.

Nevertheless, the current design is open to some improvements and optimizations. First, the promising results of this work may guide further optimization of the sensing unit design in terms of dimensions and numbers to improve the tactile probe spatial resolution. Indeed, the multiplexing capability of the FBG can be used to join together numerous sensors with smaller dimensions to reduce the encumbrance of the probe. The optimization in terms of spatial resolution can allow the proposed probe to estimate the size and stiffness of a lump in breast tissue. Moreover, the multiplexing capacity will also be exploited to add a nonencapsulated FBG to the final design for performing T compensation. Finally, to date, the proposed device can be used by applying forces on the palpated surface by performing a straight downward motion and requires to be lifted up before moving to a new location for exploring the breast surface without any feedback in terms of force or position. In the future, a control unit can be added to the proposed device with the possibility of alerting the user when exceeding a certain threshold value. However, in this

case, the reproducibility of the fabrication process must be carefully evaluated by performing a metrological assessment of the multiple sensing units to be integrated into the probe. In this way, a more accurate definition of a threshold value necessary for controlling the feedback to be sent to the user can be carried out. All these optimization steps will be necessary before moving to patients in a clinical scenario.

REFERENCES

[1] S. Najarian, J. Dargahi, and A. A. Mehrizi, *Artificial Tactile Sensing in Biomedical Engineering*. McGraw-Hill, 2009.

[2] P. Puangmali, K. Althoefer, L. D. Seneviratne, D. Murphy, and P. Dasgupta, "State-of-the-art in force and tactile sensing for minimally invasive surgery," *IEEE Sensors J.*, vol. 8, no. 4, pp. 371–380, Apr. 2008, doi: 10.1109/JSEN.2008.917481.

[3] C.-H. Won, J.-H. Lee, and F. Saleheen, "Tactile sensing systems for tumor characterization: A review," *IEEE Sensors J.*, vol. 21, no. 11, pp. 12578–12588, Jun. 2021, doi: 10.1109/JSEN.2021.3078369.

[4] A. M. Teixeira and P. Martins, "A review of bioengineering techniques applied to breast tissue: Mechanical properties, tissue engineering and finite element analysis," *Frontiers Bioeng. Biotechnol.*, vol. 11, Apr. 2023, Art. no. 1161815, doi: 10.3389/fbioe.2023.1161815.

[5] C. E. DeSantis et al., "Breast cancer statistics, 2019," *CA, Cancer J. Clinicians*, vol. 69, no. 6, pp. 438–451, Nov. 2019, doi: 10.3322/caac.21583.

[6] M. M. Koo, C. von Wagner, G. A. Abel, S. McPhail, G. P. Rubin, and G. Lyratzopoulos, "Typical and atypical presenting symptoms of breast cancer and their associations with diagnostic intervals: Evidence from a National Audit of Cancer diagnosis," *Cancer Epidemiol.*, vol. 48, pp. 140–146, Jun. 2017, doi: 10.1016/j.canep.2017.04.010.

[7] J. G. Elmore, K. Armstrong, C. D. Lehman, and S. Fletcher, "Screening for breast cancer," *JAMA*, vol. 293, no. 10, pp. 1245–1256, 2005, doi: 10.1001/jama.293.10.1245.

[8] H. Madjar, H. A. Ladner, W. Sauerbrei, A. Oberstein, H. Prömpeler, and A. Pfleiderer, "Preoperative staging of breast cancer by palpation, mammography and high-resolution ultrasound," *Ultrasound Obstetrics Gynecol.*, vol. 3, no. 3, pp. 185–190, May 1993, doi: 10.1046/j.1469-0705.1993.03030185.x.

[9] S. S. Coughlin and D. U. Ekwueme, "Breast cancer as a global health concern," *Cancer Epidemiol.*, vol. 33, no. 5, pp. 315–318, Nov. 2009, doi: 10.1016/j.canep.2009.10.003.

[10] T. McCready, D. Littlewood, and J. Jenkinson, "Breast self-examination and breast awareness: A literature review," *J. Clin. Nursing*, vol. 14, no. 5, pp. 570–578, May 2005, doi: 10.1111/j.1365-2702.2004.01108.x.

[11] A. B. Miller and C. J. Baines, "The role of clinical breast examination and breast self-examination," *Preventive Med.*, vol. 53, no. 3, pp. 118–120, Sep. 2011, doi: 10.1016/j.ypmed.2011.05.001.

[12] D. Saslow et al., "Clinical breast examination: Practical recommendations for optimizing performance and reporting," *CA, Cancer J. Clinicians*, vol. 54, no. 6, pp. 327–344, Nov. 2004, doi: 10.3322/canjclin.54.6.327.

[13] N.-J. Park, D.-H. Kang, and M. T. Weaver, "Objective and subjective breast cancer risk: Relationships with natural killer cell activity and psychological distress in healthy women," *Cancer Nursing*, vol. 33, no. 6, pp. 411–420, Nov. 2010, doi: 10.1097/NCC.0b013e3181dc37a1.

[14] W. Alomaim, D. O'Leary, J. Ryan, L. Rainford, M. Evanoff, and S. Foley, "Subjective versus quantitative methods of assessing breast density," *Diagnostics*, vol. 10, no. 5, p. 331, May 2020, doi: 10.3390/diagnostics10050331.

[15] P. S. Wellman, R. D. Howe, E. Dalton, and K. A. Kern, "Breast tissue stiffness in compression is correlated to histological diagnosis," Harvard BioRobotics Lab., Boston, MA, USA, Tech. Rep. 1, 1999.

[16] A. Samani, J. Bishop, C. Luginbuhl, and D. B. Plewes, "Measuring the elastic modulus of ex vivo small tissue samples," *Phys. Med. Biol.*, vol. 48, no. 14, pp. 2183–2198, Jul. 2003, doi: 10.1088/0031-9155/48/14/310.

[17] V. Egorov and A. P. Sarvazyan, "Mechanical imaging of the breast," *IEEE Trans. Med. Imag.*, vol. 27, no. 9, pp. 1275–1287, Sep. 2008, doi: 10.1109/TMI.2008.922192.

[18] Y. Murayama et al., "Development of a new instrument for examination of stiffness in the breast using haptic sensor technology," *Sens. Actuators A, Phys.*, vol. 143, no. 2, pp. 430–438, May 2008, doi: 10.1016/j.sna.2007.11.035.

[19] T. Erdogan, "Fiber grating spectra," *J. Lightw. Technol.*, vol. 15, no. 8, pp. 1277–1294, Aug. 1997, doi: 10.1109/50.618322.

[20] M. R. Khosravani and T. Reinicke, "3D-printed sensors: Current progress and future challenges," *Sens. Actuators A, Phys.*, vol. 305, Apr. 2020, Art. no. 111916, doi: 10.1016/j.sna.2020.111916.

[21] T. D. Ngo, A. Kashani, G. Imbalzano, K. T. Q. Nguyen, and D. Hui, "Additive manufacturing (3D printing): A review of materials, methods, applications and challenges," *Compos. B, Eng.*, vol. 143, pp. 172–196, Jun. 2018, doi: 10.1016/j.compositesb.2018.02.012.

[22] T. Li, C. Shi, and H. Ren, "A high-sensitivity tactile sensor array based on fiber Bragg grating sensing for tissue palpation in minimally invasive surgery," *IEEE/ASME Trans. Mechatronics*, vol. 23, no. 5, pp. 2306–2315, Oct. 2018, doi: 10.1109/TMECH.2018.2856897.

[23] C. Shi, M. Li, C. Lv, J. Li, and S. Wang, "A high-sensitivity fiber Bragg grating-based distal force sensor for laparoscopic surgery," *IEEE Sensors J.*, vol. 20, no. 5, pp. 2467–2475, Mar. 2020, doi: 10.1109/JSEN.2019.2951782.

[24] J. Li, C. Wang, Z. Mao, Y. Liu, Z. Wang, and H. Liu, "A compact FBG-based triaxial force sensor with parallel helical beams for robotic-assisted surgery," *IEEE Trans. Instrum. Meas.*, vol. 71, pp. 1–9, 2022, doi: 10.1109/TIM.2022.3183672.

[25] D. Lo Presti et al., "Fiber Bragg gratings for medical applications and future challenges: A review," *IEEE Access*, vol. 8, pp. 156863–156888, 2020, doi: 10.1109/ACCESS.2020.3019138.

[26] A. Abushagur, N. Arsad, M. Reaz, and A. Bakar, "Advances in bio-tactile sensors for minimally invasive surgery using the fibre Bragg grating force sensor technique: A survey," *Sensors*, vol. 14, no. 4, pp. 6633–6665, Apr. 2014, doi: 10.3390/s140406633.

[27] M. Fernandez-Vicente, W. Calle, S. Ferrandiz, and A. Conejero, "Effect of infill parameters on tensile mechanical behavior in desktop 3D printing," *3D Printing Additive Manuf.*, vol. 3, no. 3, pp. 183–192, Sep. 2016, doi: 10.1089/3dp.2015.0036.

[28] L. Avellar, C. A. F. Marques, A. Frizera, and A. Leal-Junior, "Rubber vulcanisation method for FBG sensors integration," *Opt. Fiber Technol.*, vol. 80, Oct. 2023, Art. no. 103444, doi: 10.1016/j.yofte.2023.103444.

[29] R. Min, B. Ortega, and C. Marques, "Fabrication of tunable chirped mPOF Bragg gratings using a uniform phase mask," *Opt. Exp.*, vol. 26, no. 4, p. 4411, Feb. 2018, doi: 10.1364/oe.26.004411.

[30] A. Leal-Junior et al., "Fiber Bragg gratings in CYTOP fibers embedded in a 3D-printed flexible support for assessment of human–robot interaction forces," *Materials*, vol. 11, no. 11, p. 2305, Nov. 2018, doi: 10.3390/MA11112305.

[31] A. Leal-Junior, J. Casas, C. Marques, M. Pontes, and A. Frizera, "Application of additive layer manufacturing technique on the development of high sensitive fiber Bragg grating temperature sensors," *Sensors*, vol. 18, no. 12, p. 4120, Nov. 2018, doi: 10.3390/S18124120.

[32] D. Lo Presti et al., "A wearable flower-shaped sensor based on fiber Bragg grating technology for in-vivo plant growth monitoring," *IEEE Sensors J.*, vol. 23, no. 8, pp. 8416–8425, Apr. 2023, doi: 10.1109/JSEN.2023.3253782.

[33] S. M. Desai, R. Y. Sonawane, and A. P. More, "Thermoplastic polyurethane for three-dimensional printing applications: A review," *Polym. Adv. Technol.*, vol. 34, no. 7, pp. 2061–2082, Jul. 2023, doi: 10.1002/pat.6041.

[34] T. Xu, W. Shen, X. Lin, and Y. M. Xie, "Mechanical properties of additively manufactured thermoplastic polyurethane (TPU) material affected by various processing parameters," *Polymers*, vol. 12, no. 12, pp. 1–16, Dec. 2020, doi: 10.3390/polym12123010.

[35] D. L. Presti et al., "The effect of infill pattern and density on the response of 3-D-printed sensors based on FBG technology," *IEEE Sensors J.*, vol. 22, no. 20, pp. 19357–19365, Oct. 2022, doi: 10.1109/JSEN.2022.3202101.

[36] D. Lo Presti, D. Bianchi, C. Massaroni, A. Gizzi, and E. Schena, "A soft and skin-interfaced smart patch based on fiber optics for cardiorespiratory monitoring," *Biosensors*, vol. 12, no. 6, p. 363, May 2022, doi: 10.3390/bios12060363.

[37] *Rubber, Vulcanized or Thermoplastic—Determination of Compression Stress-Strain Properties*, ISO Standard 7743:2011, 2011. Accessed: Aug. 25, 2020. [Online]. Available: https://www.iso.org/standard/72784.html

[38] F. De Tommasi, C. Romano, D. Lo Presti, C. Massaroni, M. Carassiti, and E. Schena, "FBG-based soft system for assisted epidural anesthesia: Design optimization and clinical assessment," *Biosensors*, vol. 12, no. 8, p. 645, Aug. 2022, doi: 10.3390/bios12080645.

[39] L. Xiong, G. Jiang, Y. Guo, and H. Liu, "A three-dimensional fiber Bragg grating force sensor for robot," *IEEE Sensors J.*, vol. 18, no. 9, pp. 3632–3639, May 2018, doi: 10.1109/JSEN.2018.2812820.
[40] A. G. Leal-Junior, C. Marques, M. R. N. Ribeiro, M. J. Pontes, and A. Frizera, "FBG-embedded 3-D printed ABS sensing pads: The impact of infill density on sensitivity and dynamic range in force sensors," *IEEE Sensors J.*, vol. 18, no. 20, pp. 8381–8388, Oct. 2018, doi: 10.1109/JSEN.2018.2866689.
[41] D. L. Presti et al., "An fMRI compatible smart device for measuring palmar grasping actions in newborns," *Sensors*, vol. 20, no. 21, pp. 1–16, Oct. 2020, doi: 10.3390/s20216040.
[42] *Bexa | No Woman Left Behind*. Accessed: Aug. 11, 2023. [Online]. Available: https://www.mybexa.com/?region=usa
[43] *IcosaMed's Smart Bra for Breast Cancer Monitoring Homepage*. Accessed: Aug. 11, 2023. [Online]. Available: https://icosamed.com/

D. Lo Presti (Member, IEEE) received the Ph.D. degree from UCBM, Rome, Itlay, in 2021.

She is currently an Assistant Professor with the Unit of Measurements and Biomedical Instrumentation, Università Campus Bio-Medico di Roma, Rome, Italy. Her main research activities focus on the design, fabrication, and feasibility assessment of smart systems and wearables based on fiber optics for biomedical applications.

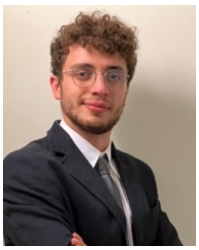

A. Dimo (Student Member, IEEE) received the M.Sc. degree from UCBM, Rome, Itlay, in 2022.

He is a Scientific Research Collaborator with the Unit of Measurements and Biomedical Instrumentation, Università Campus Bio-Medico di Roma, Rome, Italy. His research interests include the design and development of fiber Bragg grating (FBG)-based systems for biomedical applications.

L. Zoboli received the Ph.D. degree from the Università degli Studi di Roma, Rome, Italy, in 2022.

He is a Postdoctoral Researcher of Solid and Structural Mechanics with the Università Campus Bio-Medico di Roma, Rome, Italy. He is currently investigating nonlinear coupled phenomena during the curing phase of polymers. His research activity focuses on polymer modeling, multiscale mechanics, coupled physics, nuclear fusion, and finite-element analysis.

Dr. Zoboli is a member of AIMETA and Indam-GNFM.

D. Bianchi received the Ph.D. degree from the Università degli Studi di Roma, Rome, Italy, in 2017.

He is an Assistant Professor with the Università Campus Bio-Medico di Roma, Rome, Italy. His main research interests include the mathematical modeling and computational analysis of tissue biomechanics, and growth and remodeling of soft tissues.

C. Massaroni (Senior Member, IEEE) received the Ph.D. degree from UCBM, Rome, Itlay, in 2017.

He is an Assistant Professor with the Unit of Measurements and Biomedical Instrumentation, Università Campus Bio-Medico di Roma, Rome, Italy. His research interests include the design, development, and test of wearable devices and unobtrusive measuring systems for medical applications.

Dr. Massaroni has been the Chair of the "Wearable Sensors" TC of the Italy Chapter of the IEEE Sensors Council since 2020.

V. Altomare is a Full Professor of General Surgery with the Breast Surgery Unit, Campus Bio-Medico University of Rome, Rome, Italy. He is also the Director of the Breast Surgery Unit, Campus Bio-Medico Hospital Foundation, Rome. His main research interests include breast cancer management and oncoplastic surgical treatment.

A. Grasso received the Ph.D. degree from UCBM, Rome, Itlay, in 2019.

She is a Consultant Breast Surgeon with Breast Surgery Unit, Campus Bio-Medico University Hospital Foundation, Rome, Italy. Her main field of interest is the prevention, diagnosis, and treatment of breast diseases. Her research interests include oncoplastic surgery and targeted surgical therapies.

C. M. Oddo (Senior Member, IEEE) received the Ph.D. degree from Scuola Superiore Sant'Anna, Pisa, Italy, in 2011.

He is an Associate Professor with the Biorobotics Institute, Department of Excellence in Robotics and AI, and the Interdisciplinary Research Center Health Science of Scuola Superiore Sant'Anna, Pisa, Italy. He is the Head of the Neuro-Robotic Touch Laboratory, Shenzhen, China, a group with about 20 researchers. His main scientific interests are in investigating the physiological mechanisms of touch sense and in translating this body of knowledge into engineered artifacts.

A. Gizzi (Senior Member, IEEE) received the Ph.D. degree from UCBM, Rome, Itlay, in 2012.

He is an Associate Professor of Solid and Structural Mechanics with the Università Campus Bio-Medico di Roma, Rome, Italy. His main research interests include theoretical and computational biomechanics and mechanobiology.

Dr. Gizzi has been a member of the Executive Board of the European Society of Biomechanics—Italy Chapter and IEEE-EMBS since 2023.

E. Schena (Senior Member, IEEE) received the Ph.D. degree from UCBM, Rome, Itlay, in 2007.

He is a Full Professor of Measurements with the Università Campus Bio-Medico di Roma, Rome, Italy. His research interests include the design and assessment of wearable.

Dr. Schena became the Chair of the Italy Chapter of the IEEE Sensors Council in 2018.

Open Access funding provided by 'Università "Campus Bio-Medico" di Roma' within the CRUI CARE Agreement